Drug Design, Development and Therapy Dovepress

Open Access Full Text Article ORIGINAL RESEARCH

Catalpol Enhances Osteogenic Differentiation of Human Periodontal Stem Cells and Modulates Periodontal Tissue Remodeling in an Orthodontic Tooth Movement Rat Model

Jing Hu, Yang Song, Yuxing Zhang, Peng Yang, Siyu Chen, Zhaoyan Wu, Jun Zhang

Department of Orthodontics, School and Hospital of Stomatology, Cheeloo College of Medicine, Shandong University & Shandong Key Laboratory of Oral Tissue Regeneration & Shandong Engineering Research Center of Dental Materials and Oral Tissue Regeneration & Shandong Provincial Clinical Research Center for Oral Diseases, Jinan, Shandong, People's Republic of China

Correspondence: Jun Zhang, Department of Orthodontics, School and Hospital of Stomatology, Cheeloo College of Medicine, Shandong University & Shandong Key Laboratory of Oral Tissue Regeneration & Shandong Engineering Research Center of Dental Materials and Oral Tissue Regeneration & Shandong Provincial Clinical Research Center for Oral Diseases, No. 44-1 Wenhua Road West, Jinan, Shandong, 250012, People's Republic of China, Tel +86 13953109816, Fax +86 53188382923, Email zhangj@sdu.edu.cn

Purpose: This study examines the effects and mechanisms of catalpol (CAT) on the proliferation and osteogenic differentiation of cultured human periodontal ligament stem cells (hPDLSCs) in vitro and assesses the impact of CAT on periodontal remodeling in vivo using an orthodontic tooth movement (OTM) model in rats.

Methods: hPDLSCs were cultured in a laboratory setting, and their proliferation and osteogenic differentiation were assessed using the Cell-counting Kit-8 (CCK-8), Alizarin Red Staining (ARS), quantitative calcium assay, alkaline phosphatase (ALP) staining and activity assay, and immunofluorescence assay. Additionally, the expression of collagen type 1 (COL-1), ALP, and runt-related transcription factor-2 (RUNX-2) was evaluated through qRT-PCR and Western blot analysis. To verify the function of the estrogen receptor-α (ER-α)-mediated phosphatidylinositol-3-kinase-protein kinase B (PI3K/AKT) pathway in this mechanism, LY294002 (a PI3K signaling pathway inhibitor) and the ER-α specific inhibitor methyl-piperidine-pyrazole (MPP) were used. The osteogenic markers ER-α, AKT, and p-AKT (phosphoprotein kinase B) were identified through Western blot analysis. Eighteen male Sprague-Dawley rats were assigned to two groups randomly: a CAT group receiving CAT and a control group receiving an equivalent volume of saline. Micro-computed tomography (micro-CT) analysis was employed to evaluate tooth movement and changes in alveolar bone structure. Morphological changes in the periodontal tissues between the roots were investigated using hematoxylin and eosin (HE) staining and tartaric-resistant acid phosphatase (TRAP) staining. The expression of COL-1, RUNX-2, and nuclear factor-κB (NF-κB) ligand (RANKL) was assessed through immunohistochemical staining (IHC) to evaluate periodontal tissue remodeling. Tests were analyzed using GraphPad Prism 8 software. Differences among more than two groups were analyzed by one-way or two-way analysis of variance (ANOVA) followed by the Tukey's test. Values of $p < 0.05$ were regarded as statistically significant.

Results: In vitro experiments demonstrated that 10 μM CAT significantly promoted the proliferation, ALP activity, and calcium nodule formation of hPDLSCs, with a notable increase in the expression of COL-1, ALP, RUNX-2, ER-α, and p-AKT. The PI3K/AKT pathway was inhibited by LY294002, and further analysis using MPP suggested that ER-α mediated this effect. In vivo, experiments indicated that CAT enhanced the expression of COL-1 and RUNX-2 on the tension side of rat tooth roots, reduced the number of osteoclasts on the compression side, inhibited RANKL expression, and suppressed OTM.

Conclusion: CAT can promote hPDLSCs proliferation and osteogenic differentiation in vitro through the ER-α/PI3K/AKT pathway and enhance periodontal tissue remodeling in vivo using OTM models. These findings suggest the potential for the clinical application of catalpol in preventing relapse following OTM.

Keywords: catalpol, dentistry, orthodontic tooth movement, relapse, human periodontal stem cells, osteogenic differentiation, ER-α/PI3K/AKT pathway

Received: 5 August 2024
Accepted: 24 October 2024
Published: 4 November 2024

Introduction

People's pursuit of beauty gradually increases with the improvement of material living standards.[1] The treatment of malocclusion through orthodontics has also become a popular choice for achieving aesthetic goals. Orthodontic tooth movement (OTM)[2–4] refers to the response of periodontal tissue to orthodontic forces, resulting in compression ischemia-induced resorption on the pressure side and bone formation, as well as the activation of osteogenic activity on the tension side at the microscopic level. This process leads to both old bone resorption and new bone formation occurring bilaterally along the root, ultimately facilitating macroscopic tooth movement.[2,5,6] At the end of OTM, teeth tend to return to their original position or deviate, producing a new malocclusion known as relapse.[7] Many factors influence relapse, but the exact cause remains unclear.[8] It is believed that the biological mechanism of relapse[9,10] after OTM is a process of periodontal tissue remodeling, similar to OTM. Ensuring the stability of well-aligned teeth is challenging if the new bone is not formed effectively and rapidly on the original tension side. Additionally, studies have shown that the relapse rate after OTM is about 70–90%,[11] and true relapse may occur relatively soon after OTM.[12] To prevent relapse, some orthodontists recommend that patients wear retainers for as long as possible, or even for life, placing a high demand on patient compliance.[13] Therefore, promoting periodontal tissue remodeling, reducing retention time, and preventing post-orthodontic relapse have become critical issues of concern for orthodontists.[11,14]

The periodontal ligament (PDL)[15] is a supportive tissue that anchors the teeth in the jawbone, playing a vital role in tooth stability, physiological mobility, and OTM.[16] The PDL exhibits dynamic stretching properties and forms the biological basis of OTM.[2] The PDL contains a significant number of mesenchymal stromal cells (MSCs). hPDLSCs were first isolated in 2004.[17] These cells can differentiate in multiple directions, including osteogenic, adipogenic, and chondrogenic pathways. Seed cells constitute one of the three essential components of tissue engineering technology, with hPDLSCs being an ideal source of seed cells.[18,19]

CAT[20] is primarily derived from the tuberous roots of *Rehmanniae radix Praeparata* (RR), a cyclic allyl ether glucoside. RR[21] exhibits antidiabetic, cardiovascular protective, neuroprotective, anticancer, hepatoprotective, anti-inflammatory, and antioxidant effects. RR has been widely used for centuries as a traditional herbal medicine for treating bone loss induced by estrogen deficiency and is the first choice for improving bone loss in animals with osteoporosis.[22] Estrogen[23] is a crucial steroid hormone that plays an essential role in preventing osteoporosis within the human body. CAT, the sole isolated active compound from RR tested in osteoporotic animals and osteoblast models,[24–26] exhibits estrogen-like effects with a reduced risk of adverse events.[27,28]

The cellular effect of estrogen is mainly mediated by two estrogen receptors, ER-α and ER-β.[29,30] ER-α plays a crucial regulatory role in estrogen-dependent genes and bone protection.[31,32] Estrogen can mediate non-genomic signals, including activating protein/lipid kinases (eg, PI3-K, AKT, Src family kinases, MAPK family members).[31,33] The PI3K/AKT pathway[34] is a commonly encountered signaling cascade that governs various cellular biological processes, including energy metabolism, cell biosynthesis, proliferation, and differentiation. Several research investigations[35,36] have demonstrated that activating the PI3K/AKT pathway promotes the osteogenic differentiation of hPDLSCs.

Therefore, it was postulated that CAT exerts estrogen-like effects and enhances the proliferation and osteogenic differentiation of hPDLSCs in vitro via the ER-α-mediated PI3K/AKT pathway, which promotes periodontal tissue remodeling to slow down relapse after OTM. Additionally, we developed the OTM model in rats to examine the impact of CAT on periodontal remodeling in vivo.

Materials and Methods

Cultivation and Characterization of hPDLSCs

This research was undertaken in compliance with the Declaration of Helsinki and received approval from the School of Stomatology Ethics Committee at Shandong University. (No. 20,221,006). Legal guardians comprehended the study's objectives and consented to their children's participation. Premolars without dental caries or periodontal disease were collected from individuals aged 14–22 undergoing orthodontic extraction after signing informed consent forms. Extracted premolar teeth were immediately placed in α-minimum essential medium (α-MEM; Yuanpei, Shanghai, China,

containing L-glutamine, nucleosides, and deoxynucleosides) supplemented with Penicillin-Streptomycin-Gentamicin Solution (100×; Biosharp, Guangzhou, China) that was pre-cooled in advance to 4°C, and quickly transferred to the laboratory using an ice box. The solution was aspirated, and the roots were gently rinsed with phosphate-buffered saline (PBS; Solarbio, Beijing, China), which contains a 5% concentration of penicillin-streptomycin-gentamicin solution. Under sterile conditions, the periodontal ligament from the root's central region was carefully scraped off. Once the tissue blocks were affixed to the bottom of the culture flask, they were supplemented with α-MEM containing 20% (v/v) fetal bovine serum (FBS; Yeasen, Shanghai, China) and 1% (v/v) Penicillin-Streptomycin-Gentamicin Solution, followed by incubation at 37°C with 5% CO2. After approximately one week, fusiform hPDLSCs started to migrate away from the periphery of the tissue blocks. Once the cells covered about 70–80% of the lower surface of the culture flask, 2 mL of trypsin solution (Biosharp, Guangzhou, China) was added to dissociate and isolate the adherent cells. Subsequent microscopic examination revealed hPDLSCs floating and forming spherical structures. An equivalent volume of α-MEM with 10% FBS was promptly added to terminate the enzymatic digestion process. A limited dilution technique was employed to isolate and purify hPDLSCs to acquire single-cell colonies. All single-cell clones were collected for the purified hPDLSCs, and hPDLSCs between passage 3 (P3) and passage 5 (P5) were selected for a series of experiments.

Flow Cytometry

Resuspend the hPDLSCs in PBS and standardize the cell density to 1×10^7. Subsequently, 100 μL of the cell suspension was apportioned into five 1.5 mL tubes. For the control group, an equivalent volume of PBS was added to one tube, while the remaining four tubes were respectively incubated with CD34, CD44, CD45, and CD105 antibodies (Elabscience, Houston, TX, USA). All tubes were shielded from light during the incubation period. After incubating on ice for 20 minutes, the cells were washed. The flow cytometry was utilized for detection, and data analysis was conducted using FlowJo software (version 10, BD Biosciences, USA).

CCK-8 Assay

Standardize the cell density to 2×10^3 in each well of the 96-well plate. Once the cells adhered, α-MEM with CAT (purity ≥98%; Solarbio, Beijing, China) concentrations of 0, 0.1, 1, 10, 50, and 100 μM were added, with five duplicate wells set up for each concentration. After 1, 3, and 5 days of cultivation, the CCK-8 (Biosharp, Guangzhou, China) was used to measure the proliferation of hPDLSCs. Add 100 μL of α-MEM to each well containing the CCK-8 solution at a 10:1 ratio, then incubate at 37°C for 45 minutes. Measure optical density values at 450 nm with a spectrophotometer (BMG Labtech, Ortenberg, Germany).

ARS and Calcium Quantification

Standardize the cell density to 1×10^5 in each well of the 6-well plate. Once the cells adhered, they were stimulated to undergo osteogenic differentiation using an osteogenesis-inducing medium containing α-MEM with 10% FBS, 50 μg/mL ascorbic acid, 10 mm β-glycerophosphoric acid, and 0.01 μM dexamethasone. Following a 28-day induction period, the cells were rinsed thrice with PBS and then fixed with 95% ethanol. The fixative was discarded, and mineralized nodules were stained using an ARS solution (Beyotime, Shanghai, China). The nodules were examined and photographed under a microscope (Olympus Corporation, Tokyo, Japan).

For quantitative analysis of ARS, introduce a 10% (w/v) cetylpyridinium chloride (CPC) eluent and incubate for 15 minutes to achieve complete elution of alizarin red bound to the cells. Subsequently, determine the absorbance value of the eluate at OD562 nm.

Oil Red O Staining

This process employed the same cell culture technique as the previous one. An adipogenic induction medium (α-MEM with 10% FBS, 0.5 M hydrocortisone, 500 mm isobutyl methylxanthine, 60 mm indomethacin, and 10 mm insulin) was supplemented. After a 21-day induction period, the cells were washed with PBS. Following fixation with 4% formaldehyde, a drop of Oil Red O staining solution (Solarbio, Beijing, China) was added to the cell plate. The cells were examined and imaged using a microscope.

ALP Staining and ALP Activity Assay

Standardize the cell density to 5×10^4 per well in a 12-well plate. Once the cells adhered, the medium was exchanged for an osteogenesis-inducing medium. After incubating for 14 days, the cells were rinsed with PBS. Following fixation with 4% formaldehyde, a drop of BCIP/NBT Alkaline Phosphatase Colorimetric Assay Kit (Beyotime, Shanghai, China) was added to the cell plate. A darker blue color signifies increased ALP activity.

Following 14-day osteogenic induction, rinse the hPDLSCs with ice-cold PBS. The cells were treated with RIPA lysis buffer (Beyotime, Shanghai, China) containing phosphatase and protease inhibitors. The lysates were incubated at 4°C for 15 minutes, collected and centrifuged. The supernatant was then extracted for protein analysis. ALP activity was measured using the alkaline phosphatase assay kit (Solarbio, Beijing, China).

The protein concentration in the supernatant was quantified using the BCA Protein Assay Kit (Solarbio, Beijing, China). The protein solution was mixed with SDS-PAGE loading buffer (Beyotime, Shanghai, China) at a 5x concentration and heated at 100°C for 5 minutes to induce denaturation.

RNA Extraction and qRT-PCR Analysis

Following 14 days of osteogenic induction, total RNA was obtained using the Trizol method.[37] Subsequently, RNA was reverse-transcribed into complementary DNA (cDNA) through a two-step process utilizing the Strand cDNA Synthesis Kit (Yeasen, Shanghai, China). Each reaction system included five replicate wells. The primers used in this experiment were designed and analyzed as follows:

- COL-1: 5′-TAAAGGGTCACCGTGGCTTC-3′ and 5′-GGGAGACCGTTGAGTCCATC-3′
- ALP: 5′-GGCGGTGAACGAGAGAATGT-3′ and 5′-GGACGTAGTTCTGCTCGTGG-3′
- RUNX-2: 5′-GGAGTGGACGAGGCAAGAGT-3′ and 5′-AGGCGGTCAGAGAACAAACT-3′
- GAPDH: 5′-GCACCGTCAAGGCTGAGAAC-3′ and 5′-TGGTGAAGACGCCAGTGGA-3′

To quantitatively evaluate relative gene expression, the data were analyzed using the $2^{-\Delta\Delta Ct}$ method.[38] All samples were performed in triplicate, and each experiment was repeated five times.

Western Blot Analysis

Equal protein samples (20 μg/lane) separated by SDS-PAGE gels were transferred to PVDF membranes (Millipore, Merck, USA). The samples were blocked for 15 minutes at room temperature using a rapid blocking solution (Servicebio, Wuhan, China). After determining the appropriate primary antibody incubation sites based on the molecular weights of COL-1 (Proteintech, Hubei, China), ALP (Proteintech, Hubei, China), RUNX-2 (ImmunoWay, Plano, TX, USA), GAPDH (Proteintech, Hubei, China), ER-α (Abways, Shanghai, China), AKT (Abways, Shanghai, China) and p-AKT (Abways, Shanghai, China), the incubation chamber was maintained at 4°C throughout the night. The membranes were then rinsed three times with Tris-buffered saline containing 0.1% Tween 20 (TBST) (Beyotime, Shanghai, China) for 10 minutes each. The selection of secondary antibodies was based on the species of the primary antibody. After incubation, a chemiluminescent substrate (Yeasen, Shanghai, China) was used with the Chemiluminescence Imaging System (Amersham Imager 600; GE Healthcare, Little Chalfont, UK). Each experiment was repeated five times.

Immunofluorescence Assay

The treated cells were fixed at 20–25°C for 30 minutes with 4% paraformaldehyde and exposed to 0.1% Triton X-100 (Solarbio, Beijing, China) for 12 minutes. Subsequently, the cells were blocked with 5% bovine serum albumin (BSA-V; Solarbio, Beijing, China) for 1 hour and then exposed to the primary antibody for COL-1 (1:50) at 4°C throughout the night. After removing the primary antibody, the cells were incubated with the fluorescein (FITC)-conjugated affinity pure goat anti-rabbit IgG (H + L) (1:200, SA00013-2) at room temperature for 1 hour in the dark. Subsequently, the cell nuclei were stained with 4,6-diamidino-2-phenylindole (DAPI; Solarbio, Beijing, China). Observation and image capture were employed with a fluorescence microscope (Leica, Wetzlar, Germany). The fluorescence intensity was analyzed using ImageJ software (National Institutes of Health, Bethesda, MD, USA).

LY294002 and MPP Treatments

LY294002[39] is a broad-spectrum PI3K inhibitor that blocks the PI3K/AKT pathway. The cells were divided into four groups: (1) Control group: Treated with osteogenic induction medium only. (2) LY294002 group: Treated with osteogenic induction medium + 10 μM LY294002 (Soluabio, Shanghai, China). (3) CAT group: Treated with osteogenic induction medium + 10 μM CAT. (4) CAT + LY294002 group: Treated with osteogenic induction medium + 10 μM CAT + 10 μM LY294002. Upon 14 days of induction, ALP staining and Western blot analysis were executed to evaluate the expression of related proteins, whereas ARS was conducted after 28 days of induction.

MPP[40] is a selective ER-α inhibitor. The cells were divided into four groups:(1) Control group: Treated with osteogenic induction medium only. (2) MPP group: Treated with osteogenic induction medium + 10 μM MPP (Selleck, Houston, TX, USA). (3) CAT group: Treated with osteogenic induction medium + 10 μM CAT. (4) CAT + MPP group: Treated with osteogenic induction medium + 10 μM CAT + 10 μM MPP. The Western blot analysis assessed the protein expression following 14 days of induction.

Establishment of the OTM Model

Eighteen male SD rats (7 weeks old, mean weight 180±5 g, procured from Shanghai Model Organisms Ltd.) were maintained in specific pathogen-free (SPF) conditions, with a controlled temperature (20–25°C), humidity (65–70%), and a 12-hour light-dark cycle. The required experimental animal size was calculated according to the resource equation method.[41] Detailed methodology can be found in Supplementary Data 1. All experiments involving the rats adhered to the National Institutes of Health Guidelines for the Care and Use of Laboratory Animals and were approved by the Institutional Animal Care and Use Committee of Shandong University (No. 20220345).

Rats were anesthetized with the inhalational anesthetic isoflurane (Yipin Pharmaceutical Co., Ltd, Hebei, China), followed by an intraperitoneal (IP) administration of pentobarbital sodium (40 mg/kg). The orthodontic device included a nickel-titanium tension spring, stainless steel orthodontic wire (0.20 mm; Aosu, Hangzhou, China), and polymers (Charisma; Heraeus Kulzer, Germany). The right maxillary first molar was connected to the middle incisor tooth by a spring, ensuring the maxillary first molar moved towards the midline with a force of 50 g using an orthodontic dynamometer (XIHUBIOM, Hangzhou, China). After inserting the OTM device into the oral cavities of 18 rats, 9 rats were randomly allocated to the control group, receiving daily injections of an equal volume of physiological saline for the same period. In comparison, the remaining 9 rats were assigned to the CAT group and received CAT with a 10mg/kg/day dosage.

Micro-CT

The anesthetized rats were injected with 4% paraformaldehyde from the left ventricle for systemic perfusion to fix the maxillary bone tissue, specifically the right maxillary first molars. Subsequently, the samples underwent fixation in a 4% paraformaldehyde solution for 1 day at 4°C. The desiccated specimens were then affixed onto the specimen table and subjected to micro-CT scanning (Quantum GX2, PerkinElmer, USA) at 90 kV, 88 μA, each layer measuring 36 μm in thickness. The scanning region encompassed three right maxillary molars and their contiguous alveolar bone. Each specimen required approximately 15 minutes for the scanning process. Micro-CT imaging data were imported into RadiAnt Viewer software (Medixant, Poznan, Poland) in DICOM format to facilitate 3D reconstruction, with correction of each axis direction. The OTM distance was determined by measuring the shortest interproximal span between the first molar's distal surface and the second molar's mesial surface on the right maxillary.[42] The CTAn (CT analysis software; Skyscan NV) was used to compute microstructure parameters of the region of interest (ROI), including bone volume/total volume (BV/TV), trabecular thickness (Tb.Th) and trabecular separation/spacing (Tb.Sp).[43]

HE and TRAP Staining

The specimens underwent 12 weeks of decalcification in a 10% EDTA solution (pH 7.2). Decalcified specimens were subjected to progressive ethanol dehydration and embedded specimens in paraffin wax. Specimens were cut from proximal to distal direction, and the thickness of each paraffin section was 4 μm. The slides were subjected to HE

staining to observe the morphological changes in periodontal tissue. The sections performed TRAP staining with a TRAP staining kit (Solarbio, Beijing, China) to observe TRAP-positive (TRAP+) cells (osteoclasts).[44] TRAP+ cells were counted using ImageJ software.

IHC Staining

Place the slide in citrate buffer to perform high-temperature antigen retrieval. Subsequently, block non-specific binding sites with 5% goat serum for 40 minutes. Immerse the slide in a solution containing specific primary antibodies such as polyclonal anti-rabbit RUNX2 (1:200; ImmunoWay, Plano, TX, USA), COL-1 (1:300; Proteintech, Hubei, China), and RANKL (1:300; Solarbio, Beijing, China) antibodies and incubate overnight at 4°C. Incubate the biotin-labeled secondary antibody (goat anti-mouse/rabbit IgG) for a minimum of 30 minutes. Upon completion of the washing process, treat the slices using the SP reagent kit (Solarbio, Beijing, China). Following hematoxylin counterstaining, a microscopic examination of the section was performed. Use ImageJ software to determine the average optical density (AOD) value.

Data Analysis

The group assignments were concealed from the measurement personnel to ensure blinding and consistency, and the same individual conducted five repetitions for all measurements. All analyses were based on five separate experiments. Due to the small sample size per group, bootstrap was employed. The average was considered the final result. The data obtained were represented as mean ± standard deviation (mean ± SD), and one-way or two-way analysis of variance (ANOVA) was conducted using GraphPad Prism software (version 8, MacKiev Software, Boston, MA, USA). The Shapiro–Wilk test was used to evaluate the normality of the data, and the *F*-test was used to evaluate the homogeneity of the variance. The Tukey's test was used for post hoc analysis. $P < 0.05$ was considered statistically significant.

Results

Culture and Identification of hPDLSCs

At approximately 1 week of culture, spindle, and stellate cells were observed migrating out of the tissue block (Figure 1A). Individual cells were expanded in vitro for approximately 6 days to form colonies (Figure 1B), and by two weeks, the cells were uniform and spindle-shaped (Figure 1C). Lipid droplets and calcified nodules were individually observed using Oil Red O staining (Figure 1D) and ARS experimentation (Figure 1E). These results indicated that hPDLSCs can differentiate in multiple directions. Flow cytometric analysis indicated that the surface markers CD44 and CD105 (Figure 1H and J) were expressed by the MSCs associated with hPDLSCs. In contrast, the hematopoietic-related markers CD34 and CD45 (Figure 1G and I) exhibited minimal expression levels. It proved that the hPDLSCs are MSCs free from contamination by hematopoietic stem cells or endothelial cells.

Effect of CAT on Cell Proliferation

CCK-8 experiments showed that CAT (Figure 1F) at various concentrations (0, 0.1, 1, 10, 50, and 100 μM) had no significant effect on hPDLSCs on the first and third days (Figure 2). However, CAT at these concentrations stimulated the proliferation of hPDLSCs on the fifth day. Notably, CAT at various 1, 10, 50, and 100 μM concentrations significantly promoted cell proliferation ($P < 0.0001$).

Effect of CAT on ALP Activity and Calcified Nodules

ALP activity assay showed that the ALP activity of hPDLSCs induced with various concentrations of CAT (0.1, 1, 10, 50, 100 μM) was increased relative to the control group ($P < 0.0001$) (Figure 3B). According to the above results, 1, 10, and 100μM CAT were selected as low, medium, and high concentrations for follow-up experiments. ALP staining showed that the plate of 10 μM CAT was dark blue (Figure 3A). ARS showed more and darker calcified nodules in the CAT group, and the 10μM CAT group was the most apparent (Figure 3C). The calcium quantitative experiment showed the same trend as the alizarin red staining experiment ($P < 0.0001$) (Figure 3D).

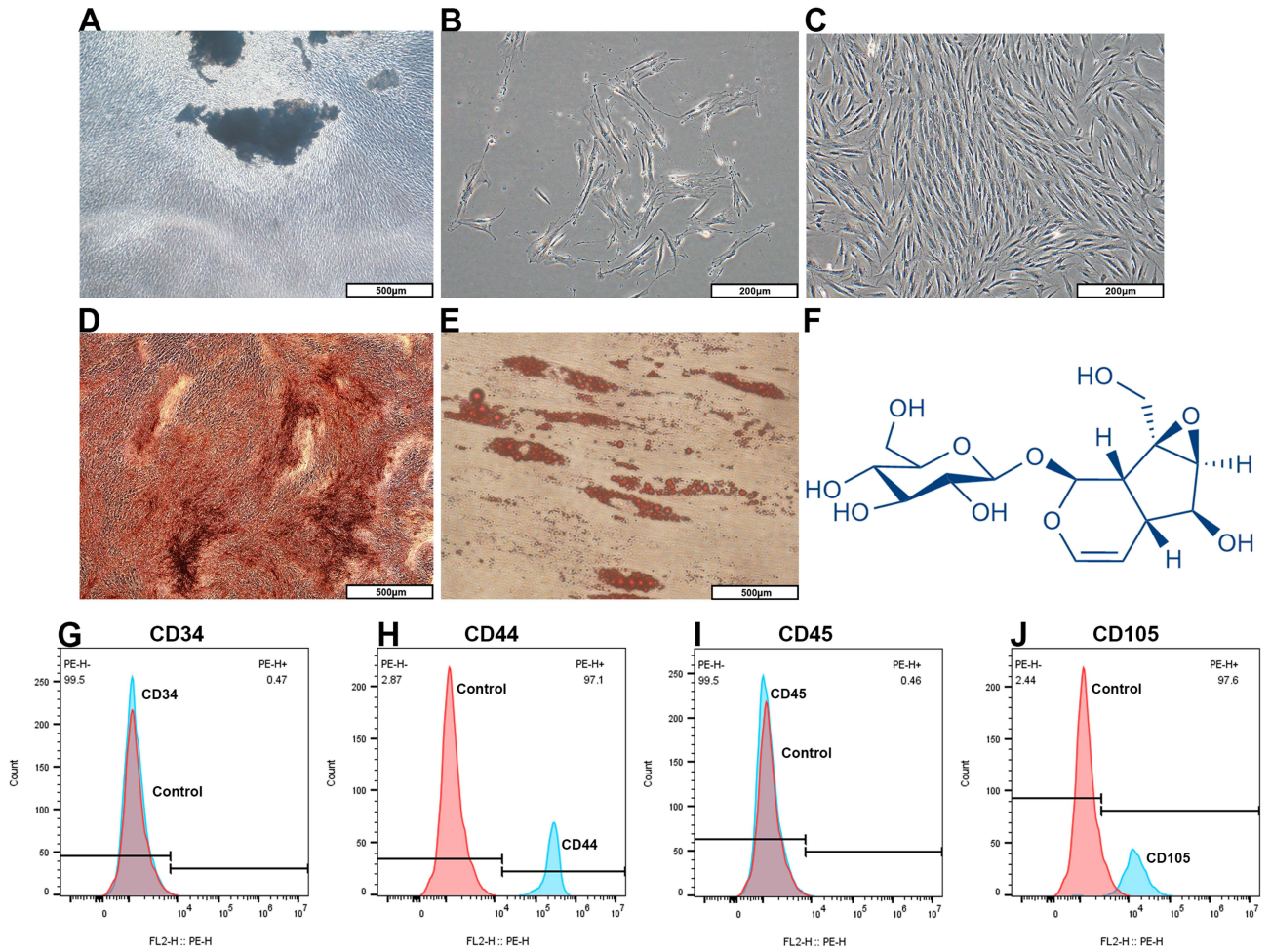

Figure 1 Cultivation and Characterization of hPDLSCs. (**A**) Stellate-shaped cells migrated out from tissue blocks. Scale bar: 500 μm. (**B**) After approximately 6 days, individual hPDLSCs formed colonies. Scale bar: 200 μm. (**C**) After about 2 weeks, hPDLSCs were arranged in a spiral pattern and exhibited a spindle-shaped morphology. Scale bar: 200 μm. (**D**) After osteogenic induction, hPDLSCs exhibited dark brown calcified nodules following Alizarin Red staining. Scale bar: 500 μm. (**E**) After adipogenic induction, hPDLSCs exhibited lipid droplets of different sizes when stained with Oil Red O. Scale bar: 500 μm. (**F**) The molecular structure of catalpol (CAT; $C_{15}H_{22}O_{10}$). (**G**–**J**) Analysis of hPDLSCs surface marker expression by flow cytometry. The expression of CD34 (**G**) and CD45 (**I**) was negative, while CD44 (**H**) and CD105 (**J**) were highly expressed.

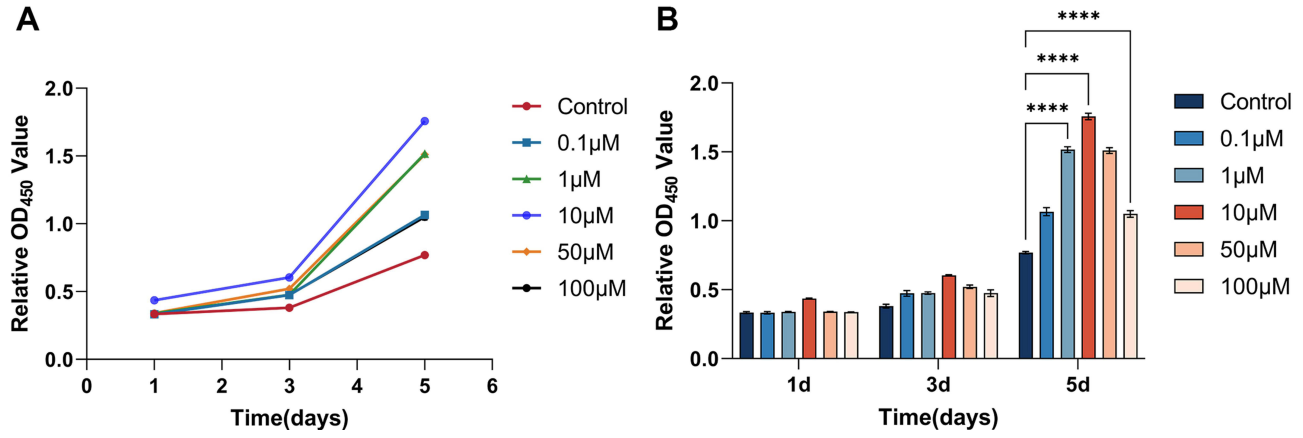

Figure 2 Effects of CAT on the proliferation of hPDLSCs. (**A** and **B**) CCK-8 analysis for the proliferation of hPDLSCs treated with CAT (0, 0.1, 1, 10, 50, 100 μM) on days 1, 3, and 5. On day 5, 10 μM CAT showed the highest proliferative activity (two-way ANOVA). Error bars stand for mean ± SD. ****$P < 0.0001$. Each experiment was repeated five times.

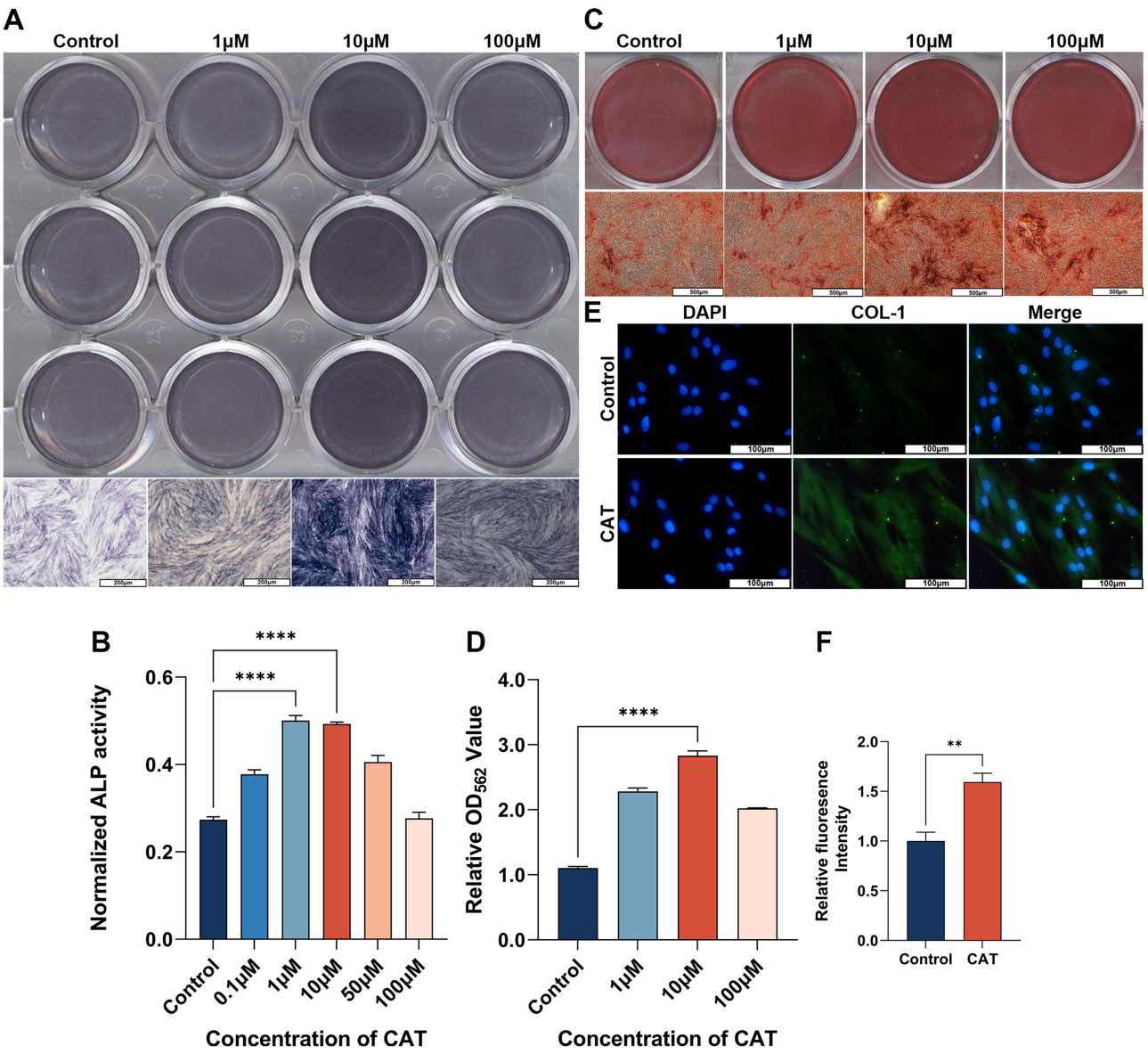

Figure 3 CAT promoted the osteogenic differentiation of hPDLSCs. (**A**) ALP staining of the plates with CAT (0, 1, 10, 100 μM). The deepest blue was observed at 10 μM CAT. Scale bar: 200 μm. (**B**) ALP activity quantification of hPDLSCs stimulated with CAT (0, 0.1, 1, 10, 50, 100 μM) for 14 days. The most significant effects were observed with 1 μM and 10 μM CAT (one-way ANOVA). Error bars stand for mean ± SD. ****$P < 0.0001$. (**C**) ARS of hPDLSCs with CAT (0, 1, 10, 100 μM) after 28 days of osteogenic induction. The deepest red was observed at 10 μM CAT with the highest number and darkest color of calcified nodules. Scale bar: 500 μm. (**D**) Quantitative determination of ARS (one-way ANOVA). Error bars stand for mean ± SD. ****$P < 0.0001$. (**E**) Immunofluorescence detection of the expression of COL-1. 10 μM CAT was observed with the strongest immunofluorescence intensity. Scale bar: 100 μm. (**F**) Quantitative detection of COL-1 immunofluorescence intensity (one-way ANOVA). Error bars stand for mean ± SD. **$P < 0.01$. Each experiment was repeated five times.

Effect of CAT on the Expression Levels of COL-1, ALP, RUNX-2, p-AKT, and ER-α

qRT-PCR showed that 1, 10, and 100 μM CAT promoted the expression of osteogenesis-related genes COL-1 (Figure 4C), ALP (Figure 4D) and RUNX-2 (Figure 4E) ($P < 0.0001$). Western blot assay (Figure 4A and B) showed that 1, 10, and 100 μM CAT promoted the expression of proteins related to osteogenesis, including COL-1 (Figure 4F), ALP (Figure 4G), RUNX-2 (Figure 4H), p-AKT (Figure 4I) ($P < 0.0001$) and ER-α ($P < 0.001$) (Figure 4J). The results aligned with the trend observed in qRT-PCR, where 10 μM CAT contributed the most. Based on these experiments, 10 μM CAT was selected as the optimal concentration for immunofluorescence staining (Figure 3E). The evidence suggested that 10 μM CAT could stimulate the expression of COL-1, and the fluorescence intensity exhibited a significant increase compared to the control group ($P < 0.01$) (Figure 3F).

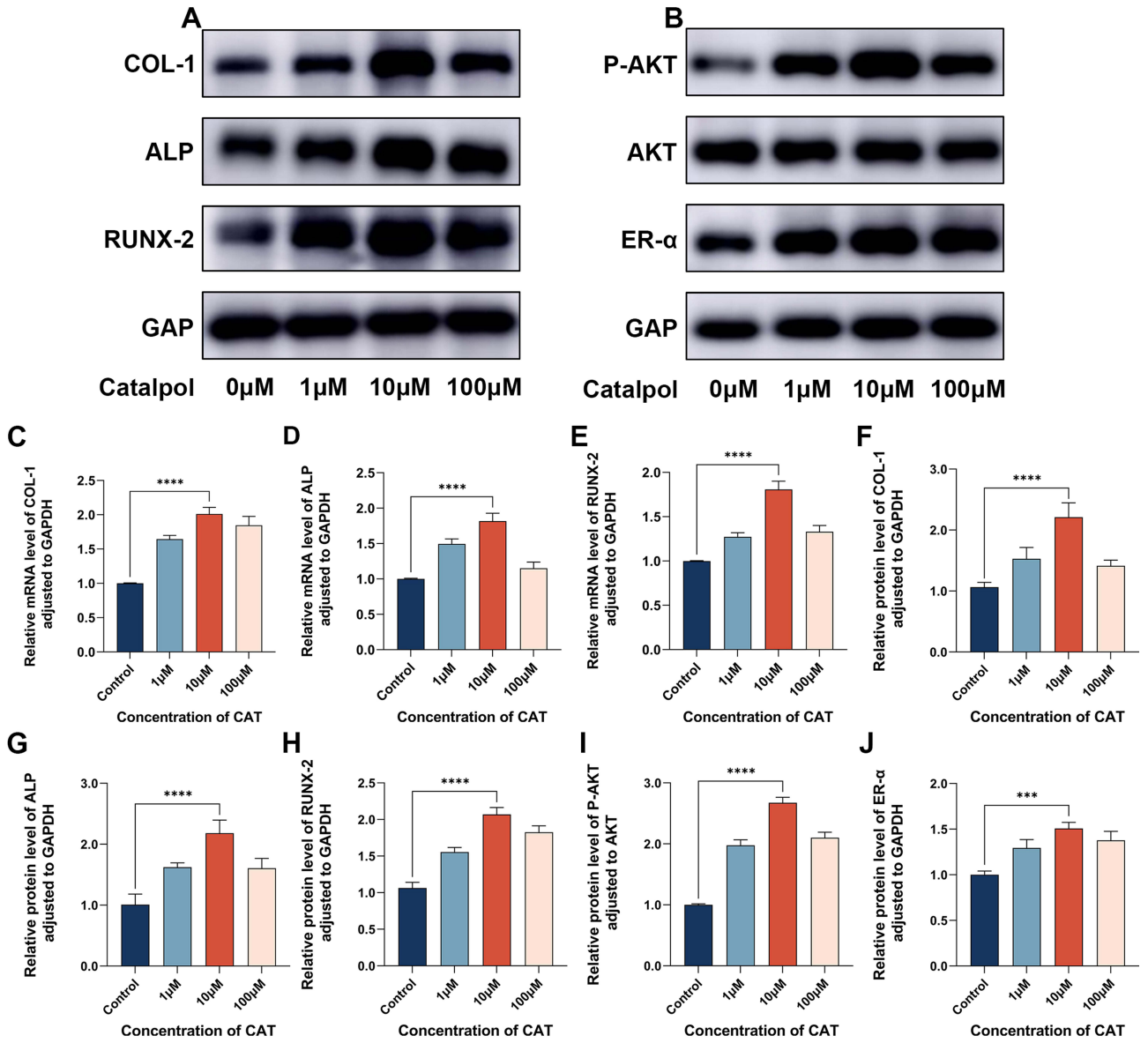

Figure 4 CAT promotes the expression of osteogenic differentiation markers in hPDLSCs. (**A**) The protein levels of COL1, ALP, and RUNX2 with CAT (0, 1, 10, 100 μM) after osteogenic induction for 14 days. (**B**) The protein levels of p-AKT and ER-α with CAT (0, 1, 10, 100 μM) after osteogenic induction for 14 days. (**C–E**) The mRNA levels of COL1, ALP, and RUNX2 with CAT (0, 1, 10, 100 μM) after osteogenic induction for 14 days (one-way ANOVA). Error bars stand for mean ± SD. ****$P < 0.0001$. (**F–J**) Relative quantification of COL1 (**F**), ALP (**G**), RUNX2 (**H**), p-AKT (**I**), and ER-α (**J**) protein levels with CAT (0, 1, 10, 100 μM) after osteogenic induction for 14 days (one-way ANOVA). Error bars stand for mean ± SD. ***$P < 0.001$, ****$P < 0.0001$. Each experiment was repeated five times.

CAT Stimulates Osteogenic Differentiation by Activating the PI3K/AKT Pathway

To further investigate the mechanism of CAT on the osteogenic differentiation of hPDLSCs, the cells were exposed to 10 μM CAT with or without LY294002. After the addition of LY294002, ALP activity (Figure 5B) was decreased ($P < 0.0001$), ALP staining (Figure 5A) and ARS (Figure 5C) became light, and calcium nodules were reduced (Figure 5D) ($P < 0.0001$). Western blot analysis (Figure 6A and B) unveiled the levels of expression for p-AKT (Figure 6F), and osteogenic-related proteins COL-1 (Figure 6C), ALP (Figure 6D), and RUNX-2 (Figure 6E) were down-regulated ($P < 0.01$, $P < 0.001$, $P < 0.0001$), indicating that the PI3K/Akt pathway was inhibited. The original osteogenic effect was also inhibited. Interestingly, however, the increased expression of ER-α (Figure 6G) due to CAT was not reversed.

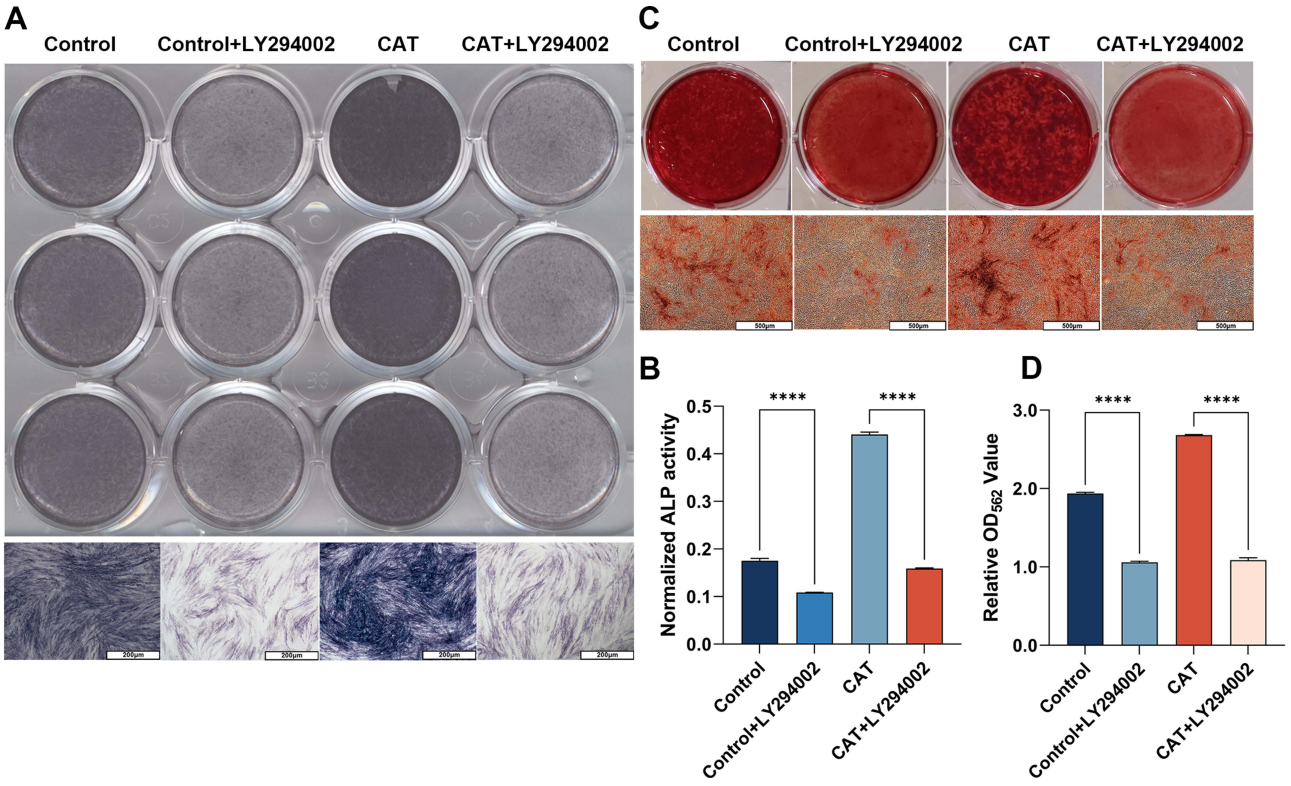

Figure 5 CAT promoted osteogenic differentiation of hPDLSCs through the PI3K/AKT pathway. LY294002 successfully reversed the promotion of ALP activity and calcium nodule formation by CAT. (**A**) ALP staining images following osteogenic induction for 14 days of the control and CAT groups (10 μM) with or without LY294002 were added. (**B**) ALP activity quantification of hPDLSCs following osteogenic induction for 14 days of the control and CAT groups (10 μM) with or without LY294002 added (one-way ANOVA). Error bars stand for mean ± SD. ****$P < 0.0001$. (**C**) Representative images of ARS after osteogenic induction for 28 days of the control group and CAT group (10 μM) with or without LY294002 added. (**D**) Quantitative determination of ARS after osteogenic induction for 28 days of the control group and CAT group (10 μM) with or without LY294002 added (one-way ANOVA). Error bars stand for mean ± SD. ****$P < 0.0001$. Each experiment was repeated five times.

ER-α Mediates Stimulation of the PI3K/AKT Pathway by CAT

Western blot analysis (Figure 7A and B) indicated that treatment of hPDLSCs with 10 μM CAT with/without MPP led to a reduction in ER-α expression ($P < 0.0001$) (Figure 7G) upon the addition of MPP. This reduction was accompanied by the down-regulation of p-AKT (Figure 7F) and the osteogenesis-associated proteins COL-1 (Figure 7C), ALP (Figure 7D), and RUNX-2 (Figure 7E) ($P < 0.01$, $P < 0.001$, $P < 0.0001$). It demonstrated that both the ER-α and PI3K/AKT pathways were inhibited, with ER-α upstream of the PI3K/AKT pathway, suggesting that ER-α plays an essential role in activating the PI3K/AKT pathway.

OTM Model and Micro-CT Analysis

The OTM model was established in rats, as shown in Figure 8A. During the experiment, the rats were in good health, and the CAT group showed no significant weight changes compared to the control group (Figure 8B), as elaborated in Supplementary Table 1. The right maxillary first molar was moved mesially after 50 g traction for 14 days, and the movement distance (Figure 8C and D) was reduced in the CAT group (10 mg/kg/day CAT) compared to the control group (saline) ($P < 0.05$). The data on each rat's tooth travel distance is shown in Supplementary Table 2. During the same period, a decrease in the speed of OTM was observed in the CAT group. On the tension side of the distal mesial buccal root of the first molar, BV/TV, Tb.Sp and Tb.Th showed an increase in the CAT group relative to the control group ($P < 0.05$, $P < 0.01$). On the pressure side, BV/TV, Tb.Sp and Tb.Th also experienced a minor increase in the CAT group; however, the disparity lacked statistical significance (Figure 8E–H).

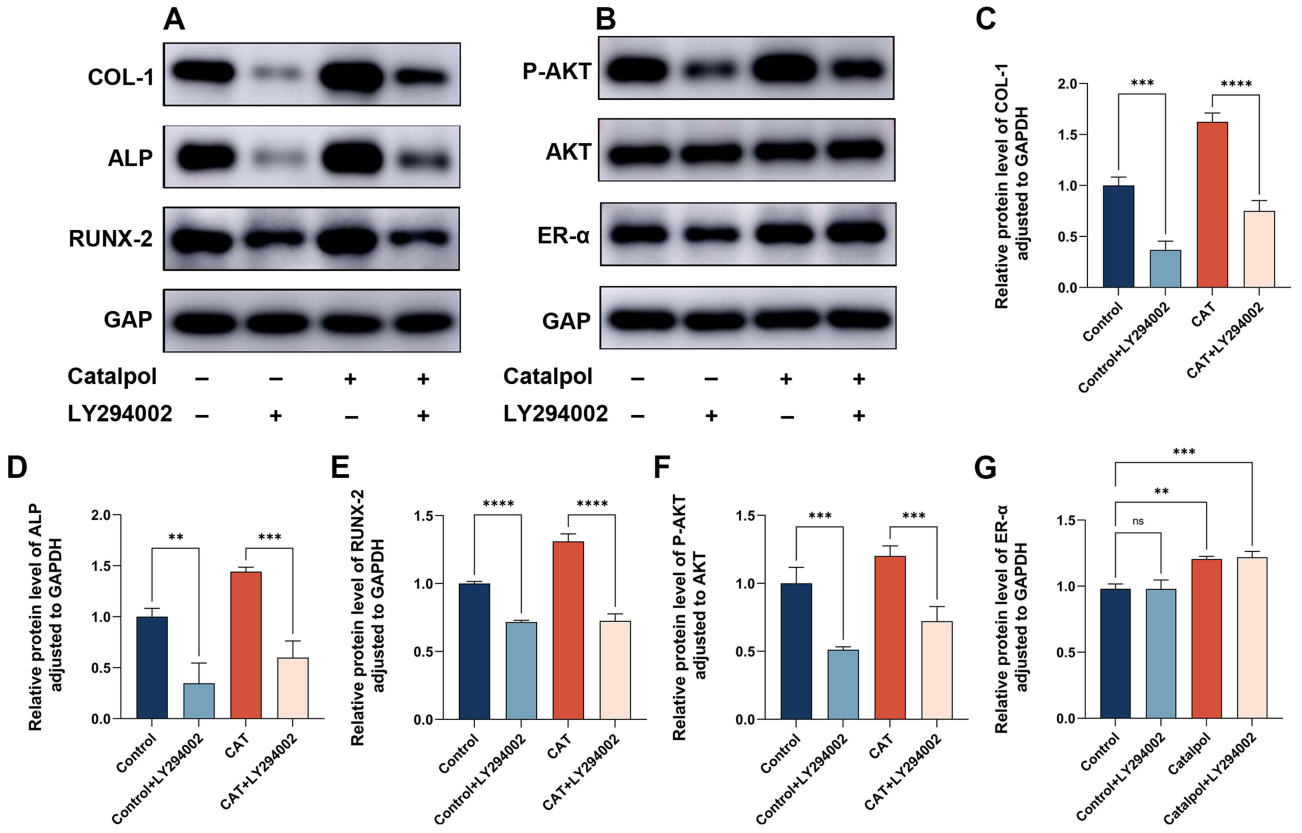

Figure 6 CAT promoted osteogenic differentiation of hPDLSCs through the PI3K/AKT pathway. LY294002 successfully reversed the expression of osteogenic differentiation markers by CAT. (**A** and **B**) The protein levels of COL1, ALP, RUNX2, p-AKT, and ER-α following osteogenic induction for 14 days of the control group and CAT group (10 μM) with or without LY294002 added. (**C**–**G**) Relative quantification of COL1 (**C**), ALP (**D**), RUNX2 (**E**), p-AKT (**F**), and ER-α (**G**) protein levels following osteogenic induction for 14 days of the control group and CAT group (10 μM) with or without LY294002 added (one-way ANOVA). Error bars stand for mean ± SD. $^{**}P < 0.01$, $^{***}P < 0.001$, $^{****}P < 0.0001$. Each experiment was repeated five times.

HE and TRAP Staining Observation

HE staining (Figure 9A) showed that the PDL of the maxillary first molar became narrower on the pressure side, while the PDL became wider on the tension side, and the cells exhibited a long spindle shape. The cellular arrangement of the control group was disturbed, whereas the cells of the CAT group were arranged in a relatively continuous and dense pattern. TRAP staining (Figure 9B) revealed positive multinucleated cells (osteoclasts) distributed on the tooth root and alveolar bone surface, with bone resorption pits surrounding the cells. Compared to the control group, the number of osteoclasts (Figure 9C) on the compressive side of the root in the CAT group decreased ($P < 0.05$).

IHC Staining Analysis

IHC staining (Figure 9D–I) was conducted to assess the immunoreactivity of COL-1, RUNX-2, and RANKL in the PDL. In the CAT group, compared to the control group, COL-1, and RUNX-2 expression increased on the tension side ($P < 0.05$, $P < 0.01$), while RANKL expression decreased on the pressure side ($P < 0.05$).

Discussion

hPDLSCs are regarded as the primary and reliable cells for periodontal tissue regeneration, forming the foundation for filling periodontal tissue defects through cell and gene therapy.[45,46] Among the available stem cells, hPDLSCs are easily obtained and less invasive to the donor.[17] This investigation achieved the successful isolation and cultivation of hPDLSCs. Flow cytometry analysis confirmed that hPDLSCs are ectomesenchymal stem cells, free from contamination by hematopoietic stem cells and endothelial cells. In vitro induction of hPDLSCs resulted in lipid droplets and calcified nodules forming, demonstrating their multi-directional differentiation capacity. Studies have shown that hUCMSC-

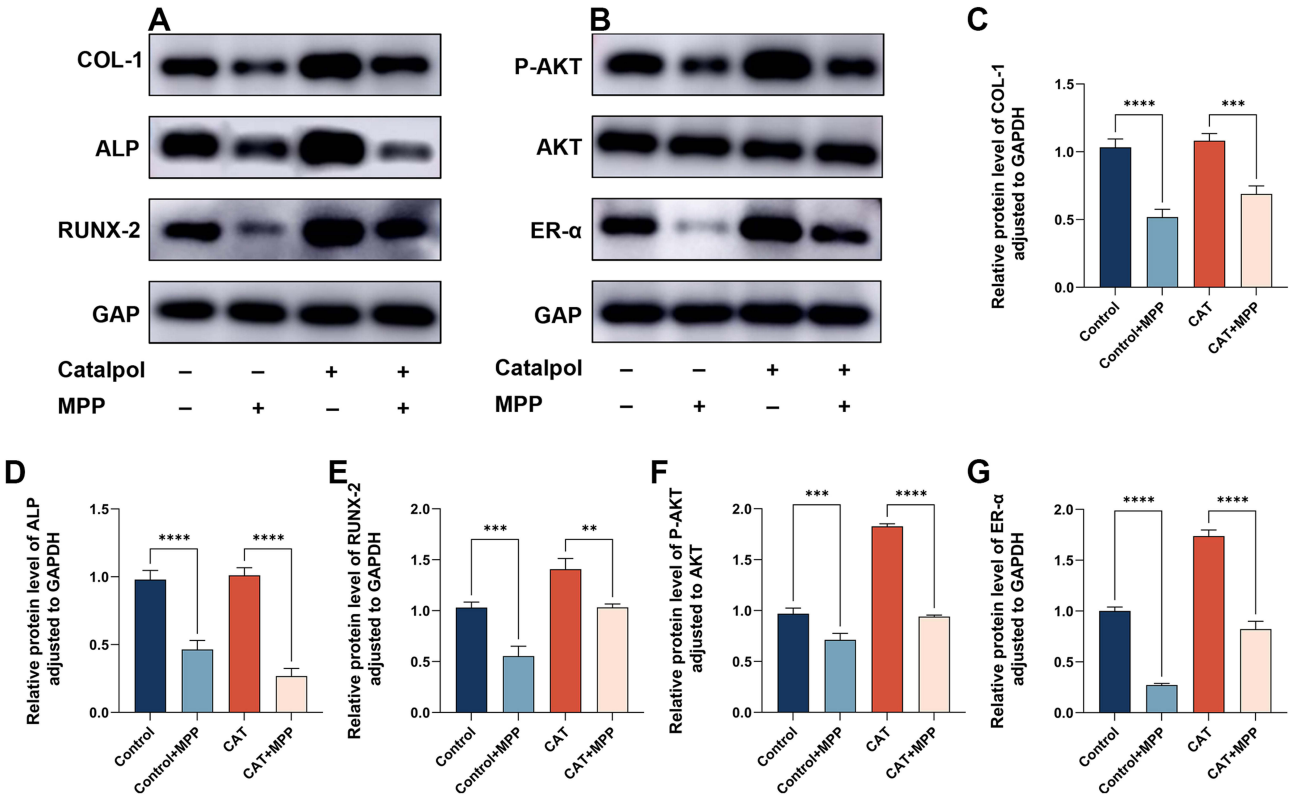

Figure 7 CAT activated the PI3K/AKT pathway mediated by ER-α to promote the osteogenic differentiation of hPDLSCs. MPP successfully reversed the expression of osteogenic differentiation and pathway-related markers by CAT. (**A** and **B**) The protein levels of COL1, ALP, RUNX2, p-AKT, and ER-α following osteogenic induction for 14 days of the control group and CAT group (10 μM) with or without MPP added. (**C**–**G**) Relative quantification of COL1 (**C**), ALP (**D**), RUNX2 (**E**), p-AKT (**F**), and ER-α (**G**) protein levels following osteogenic induction for 14 days of the control group and CAT group (10 μM) with or without MPP added (one-way ANOVA). Error bars stand for mean ± SD. $^{**}P < 0.01$, $^{***}P < 0.001$, $^{****}P < 0.0001$. Each experiment was repeated five times.

exosomes activated the PI3K/AKT pathway to facilitate osteogenic differentiation in hPDLSCs under hyperglycemic conditions.[47] Han et al revealed that Ipriflavone stimulates osteogenic differentiation of hPDLSCs through the GPR30/PI3K/AKT pathway.[48] hPDLSCs represent a real potential for regenerating periodontal tissues, both for the orthodontic treatment of patients with periodontitis and for the retention phase after OTM.

Estrogen stimulates osteogenic differentiation of hPDLSCs, inhibits osteoclastic differentiation, promotes apoptosis, and regulates periodontal tissue remodeling in OTM.[30] Phytoestrogens, such as CAT, have minimal adverse reactions, in contrast to the rare but significant side effects associated with estrogen use for preventing osteoporosis in postmenopausal women, which include jawbone necrosis, atypical fractures, breast cancer, and thromboembolism.[49,50] On January 25, 2017, "Catalpol Tablet",[21] a traditional Chinese medicinal product, received clinical research approval from the State Food and Drug Administration (SFDA). Following systematic pharmacological mechanism and pharmacokinetics studies, CAT has been identified as a compound of significant medicinal value. CAT was found to promote osteogenic-angiogenic coupling and was validated in a rat model of cranial bone defects in osteoporosis.[51] Additionally, CAT ameliorates dexamethasone-induced osteoporosis by promoting osteogenic differentiation of BMSCs by activating the PKD1 promoter.[26] Therefore, CAT has excellent biological safety as a phytoestrogen involved in bone metabolism.

hPDLSCs increased levels of osteogenesis-related gene expression, such as COL-1, ALP and RUNX-2, at 14 and 21 days in an osteogenic medium.[52] In the present study, the upregulation of COL-1, ALP, and RUNX-2 expression was significant at 14 days of osteogenic induction in hPDLSCs, consistent with the above results. ALP[53] is one of the earliest functional genes in the calcification mechanism and a marker of osteoblast maturation. The 10 μM CAT group exhibited the highest ALP activity and darkest blue ALP staining. COL-1 serves as an indicator for osteogenesis and collagen formation. Mutations in the COL-1 gene can lead to osteogenesis imperfecta (OI).[54] Immunofluorescence assay of COL-1 in the 10 μM CAT group revealed a significant enhancement of fluorescence intensity. RUNX-2[55] is an essential

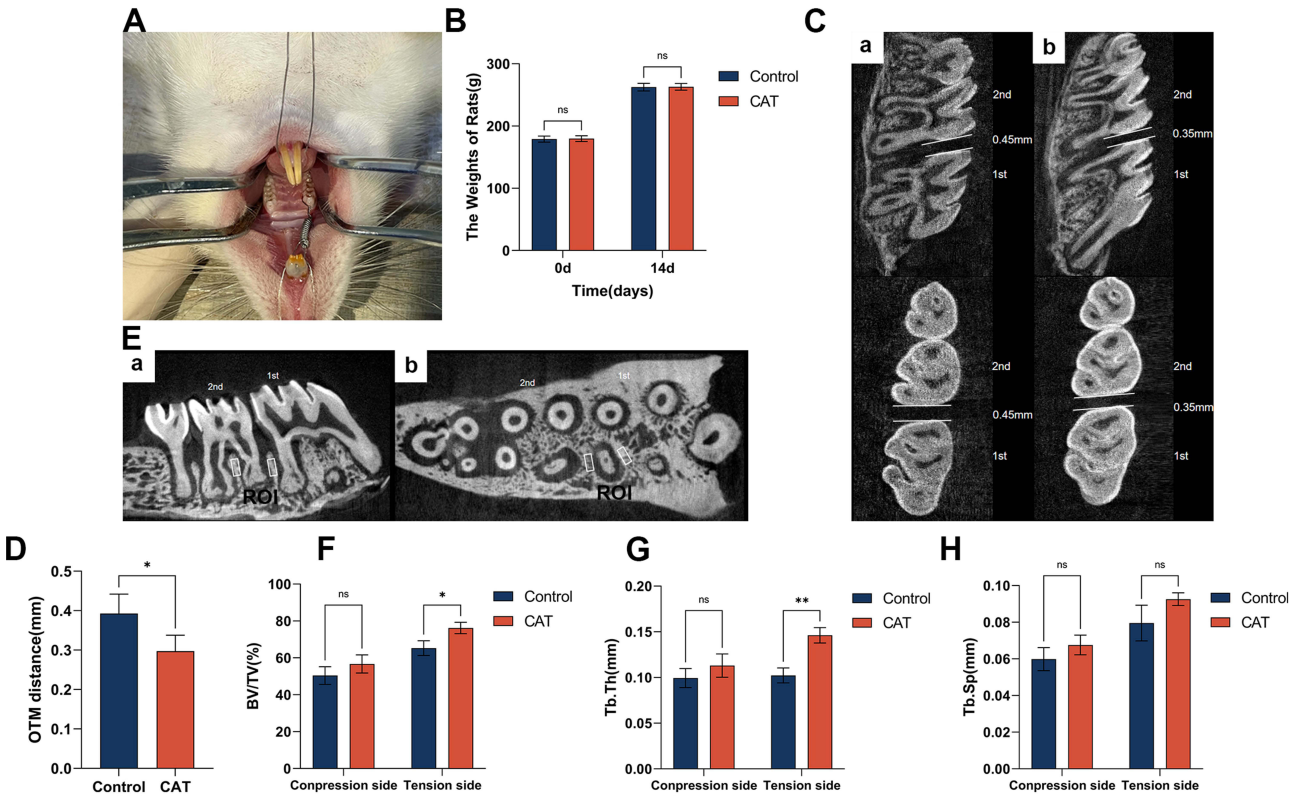

Figure 8 The establishment of the orthodontic tooth movement model and three-dimensional reconstruction analysis of sample data. (**A**) Orthodontic tooth movement model in rats. (**B**) Weight changes of rats in the control and 10mg/kg/day CAT groups at day 14 (one-way ANOVA). Error bars stand for mean ± SD (n=9). (**C**) Measurement of the mesial movement distance of the first molar on the right maxillary. Illustration of the comparison between the control (**a**) and 10mg/kg/day CAT (**b**) groups in measuring the mesial movement distance of the first molar on the right maxillary. Abbreviations: 1st, first molar; 2nd, second molar. (**D**) Quantitative analysis of the mesial displacement of the first molar on the right maxillary in the control group and 10mg/kg/day CAT group (one-way ANOVA). Error bars stand for mean ± SD (n=9). *$P < 0.05$. (**E**) Region of interest (ROI) of bone analysis marked with a white box. a, vertical view; b, horizontal view. Abbreviations: 1st, first molar; 2nd, second molar. (**F–H**) Evaluation of trabecular bone on day 14. Bone volume/total volume (BV/TV), trabecular thickness (Tb.Th), and trabecular separation (Tb.Sp) of the control group and 10mg/kg/day CAT group on the compression side and tension side (one-way ANOVA). Error bars stand for mean ± SD (n=9). *$P < 0.05$, **$P < 0.01$.

osteogenesis marker activating the osteoblast differentiation gene. RUNX-2 regulates ALP and COL-1 by binding to cis-acting elements (OSE2 in the OC promoter region), a mechanism that emphasizes the importance of RUNX-2 in studying skeletal development.[56] The occurrence of calcium nodules is a manifestation of osteogenic differentiation and maturation, reflecting the ability of late osteogenic differentiation. The results of these osteogenesis-related metrics indicated that appropriate concentrations of CAT promoted the osteogenic differentiation of hPDLSCs, with 10 μM of CAT achieving the maximum stimulation response. This finding is consistent with previous reports[57] that hPDLSCs have a hormone dose response similar to stem cells.

The PI3K/AKT pathway significantly regulates osteoblast and osteoclast function by affecting their formation, proliferation, differentiation, and apoptosis.[58] AKT activation is highly correlated with osteogenesis, as evidenced by an increase in osteogenic markers, including COL-1 and RUNX-2, which trigger the maturation of stem cells into functional osteoblasts.[36] RUNX-2 and the PI3K/AKT/mTOR pathways form a feedback loop that positively regulates the differentiation of osteoblasts.[59] It has been demonstrated that AKT activity is required at all stages of osteoblast differentiation and function, and the PI3K/AKT pathway represents a crucial element within the intricate osteogenic pathway network.[60] Previous studies[28] have found that CAT exerts antidiabetic, cardioprotective, vasoprotective, and antitumor effects closely related to the PI3K/AKT pathway. LY294002[61] is a potent inhibitor of PI3K/AKT, which reduces the expression of phosphorylated AKT (Ser473). In this study, LY294002 successfully inhibited the PI3K/AKT pathway, leading to the reversal of the estrogen-like effect produced by CAT on hPDLSCs. The decrease in ALP activity, lightening of ALP staining, reduction in calcium nodules, and decreased expression of relevant osteogenic markers all indicate that CAT stimulates the osteogenic differentiation of hPDLSCs by triggering the PI3K/AKT pathway.

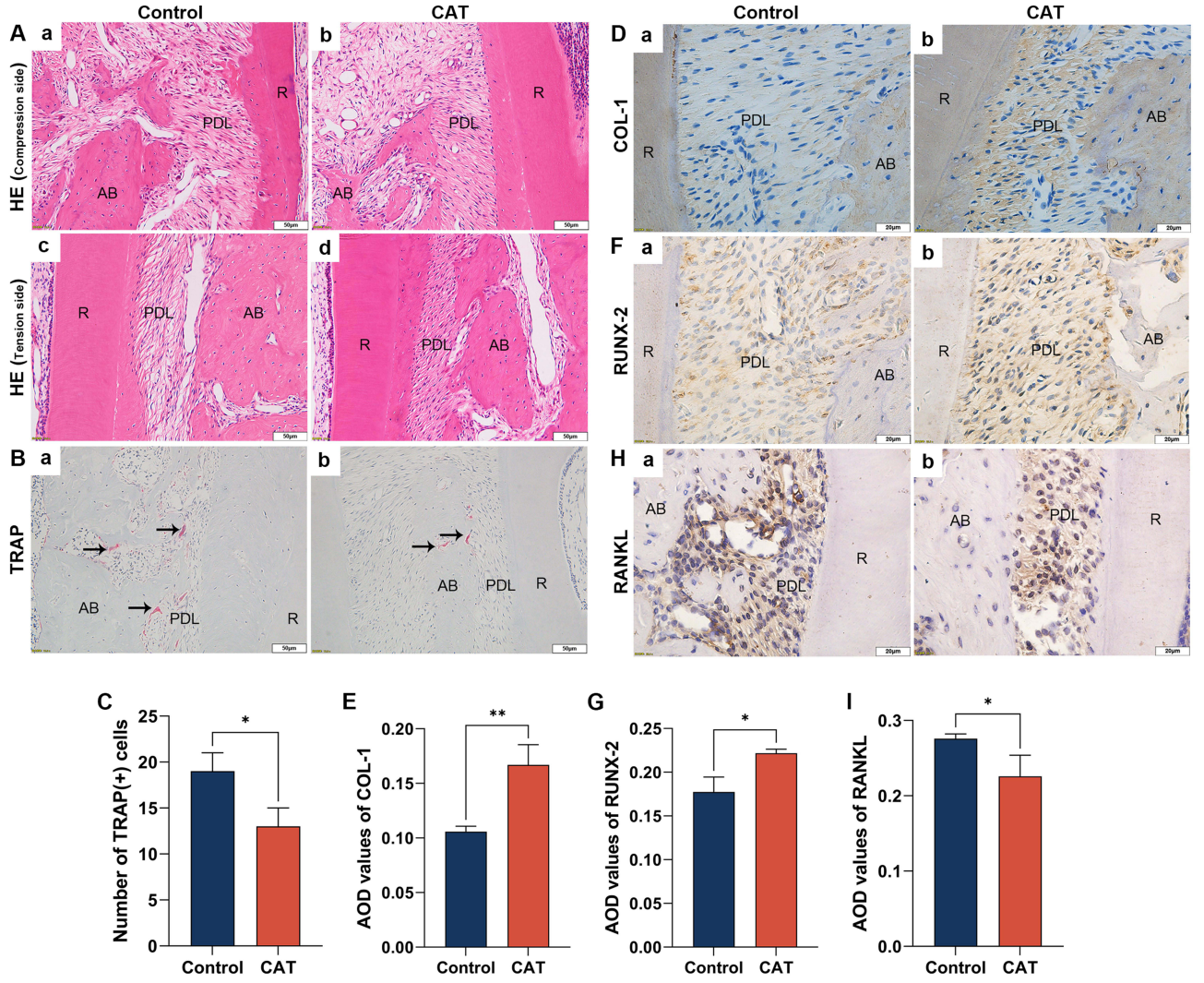

Figure 9 Results of HE, TRAP, and IHC staining. Abbreviations: AB, alveolar bone; PDL, periodontal ligament; R, root. (**A**) HE staining on the compression side of periodontal tissue in both the control group (**a**) and 10 mg/kg/day CAT group (**b**) and on the tension side of periodontal tissue in both the control group (**c**) and 10 mg/kg/day CAT group (**d**). Scale bar: 50 μm. (**B**) TRAP staining on the compression side of periodontal tissue in both the control group (**a**) and 10 mg/kg/day CAT group (**b**). TRAP-positive cells were marked by black arrows. Scale bar: 50 μm. (**C**) The number of TRAP-positive cells in the 10 mg/kg/day CAT group (**a**) decreased relative to the control group (**b**) (one-way ANOVA). Error bars stand for mean ± SD (n=9). *$P < 0.05$. (**D–I**) The immunoreactivity of COL-1 (**D**), RUNX-2 (**F**), and RANKL (**H**) in the control group (**a**) and 10 mg/kg/day CAT group (**b**) was detected after 14-day OTM, and their AOD values (**E, G** and **I**) were measured (one-way ANOVA). The expression of COL-1 (**D**) and RUNX-2 (**F**) could be observed on the tension side, while RANKL (**H**) was mainly expressed on the compression side. Scale bar: 20 μm. Error bars stand for mean ± SD (n=9). *$P < 0.05$, **$P < 0.01$.

Studies[62,63] have suggested the involvement of both ER-α and ER-β of hPDLSCs in osteogenic differentiation. Given this perspective, we selectively inhibited ER-α in hPDLSCs using MPP, which reduced the expression of ER-α, p-AKT, and related osteogenic markers. It indicates that not only do hPDLSCs express ER-α, but ER-α also regulates the osteogenic differentiation process of hPDLSCs by mediating the PI3K/AKT pathway. Wu et al[64] suggested that the phytoestrogen Genistein could improve bone healing by triggering ER-α-mediated expression of osteogenesis-related genes and subsequent osteoblast maturation. Additionally, mechanical forces can activate ER-α in hPDLSCs and affect osteogenesis and differentiation of osteoblasts;[30] therefore, activation of ER-α is essential in regulating OTM and relapse. Furthermore, it was found that regulation of ER-α expression in osteoclast precursor cells induced osteoclast apoptosis and reduced osteoclast activity and proliferation.[65] This demonstrates that ER-α is an essential regulator of bone homeostasis.

This investigation focused on exploring the impact of CAT on periodontal tissue remodeling in vivo by establishing an animal model.[42,43] Micro-CT analysis showed that BV/TV, Tb.Sp and Tb.Th increased on the tension side, suggesting

that CAT can enhance osteogenic differentiation compared to the control group. IHC staining for COL-1 and RUNX-2 also confirmed that CAT may promote osteogenic differentiation on the tension side. No significant statistical variances were noted in BV/TV, Tb.Sp and Tb.Th when compared with the control group. However, these parameters were elevated on the compression side. TRAP staining experiments demonstrated a reduction in osteoclasts on the pressure side in the CAT group compared with the control group. Thus, we inferred that CAT inhibited osteoclastic activity on the pressure side. Activating RANKL/RANK signaling stimulates osteoclast formation and differentiation, promoting bone resorption.[66] Previous research[67] has indicated that CAT suppresses osteoclastogenesis by inhibiting RANKL and the expression of osteoclast-specific genes. CAT promotes osteoclast apoptosis through the Sirt6-ER-α-FasL axis to alleviate osteoporosis in ovariectomized rats.[32] In this study, the expression of RANKL on the root pressure side of rats in the CAT group was decreased, indicating that CAT was implicated in the modulation of osteoclasts during bone remodeling, which was the same as the results of previous studies.[68] Under mechanical forces within the biological system, bone resorption occurs on the compressed side, while osteogenesis occurs on the tension side, achieving a dynamic equilibrium and enabling OTM. In vivo experiments demonstrated that CAT promotes osteogenic differentiation of periodontal tissues on the tension side and suppresses bone resorption on the compression side, ultimately reducing tooth movement distance. This provides a reference for post-orthodontic retention, tooth relapse, and displacement prevention.

Based on the above-discussed findings, we propose that 10 μM CAT effectively promotes the proliferation and osteogenic differentiation of human periodontal ligament stem cells (hPDLSCs) via the ER-α-mediated activation of the PI3K/Akt pathway. Furthermore, the administration of 10 mg/kg/day CAT exhibited significant effects on the tension side of the moving root by promoting osteogenic differentiation and simultaneously inhibiting bone resorption on the compression side, thereby positively preventing relapse after orthodontic tooth movement (OTM). Consequently, CAT holds great potential as a natural therapeutic agent for periodontal tissue regeneration and for delaying relapse after OTM.

In the context of the existing literature, our findings align with previous studies that emphasize the significance of the PI3K/Akt pathway in osteogenic differentiation and periodontal regeneration. For instance, recent research[47,48] has demonstrated that activating this pathway can enhance the regenerative capacity of various stem cells in different scenarios, supporting the notion that CAT's mechanism of action is consistent with broader evidence in regenerative medicine. Moreover, exploring the potential synergistic effects of CAT in combination with other adjunctive treatments, such as ozone therapy,[69] photobiomodulation,[70] and para probiotics,[71] would be of considerable value. Understanding these interactions could offer insights into optimizing periodontal treatment protocols and improving clinical outcomes.

However, we must admit certain limitations in our study. The results obtained from rat models might only partially apply to human applications due to differences in bone structure, drug dosage, force magnitude, and treatment duration. Additionally, the long-term effects of CAT on periodontal tissues and the potential side effects remain ambiguous, requiring further investigation. Future research should address these gaps, particularly regarding the specific dosage and treatment regimens that apply to human patients. Furthermore, the mechanisms by which CAT regulates osteoclast activity and its broader implications in bone remodeling need to be clarified. Investigating these aspects will be crucial for understanding the full therapeutic potential of CAT in periodontal therapy.

Conclusion

We demonstrated that catalpol promoted hPDLSCs proliferation and osteogenic differentiation in vitro through the ER-α/PI3K/AKT pathway and enhanced periodontal tissue remodeling in vivo using OTM models. Our research may serve as an experimental paradigm for the appropriate clinical utilization of catalpol to slow down relapse after OTM.

Abbreviations

CAT, catalpol; hPDLSCs, human periodontal ligament stem cells; OTM, orthodontic tooth movement; CCK-8, Cell-counting Kit-8; ARS, Alizarin Red Staining; ALP, alkaline phosphatase; COL-1, collagen type 1; RUNX-2, runx family transcription factor 2; qRT-PCR, quantitative reverse transcription polymerase chain reaction; ER-α, receptor-α; PI3K/AKT, phosphatidylinositol-3-kinase-protein kinase B; MPP, methyl-piperidine-pyrazole; p-AKT, phosphoprotein kinase B; micro-CT, Micro-computed tomography; HE, hematoxylin and eosin; TRAP, tartaric-resistant acid phosphatase;

RANKL, nuclear factor-κB (NF-κB) ligand; IHC, immunohistochemical; PDL, periodontal ligament; MSCs, mesenchymal stromal cells; RR, *Rehmanniae radix Praeparata*; ER-β, receptor-β; MAPK, Mitogen-Activated protein kinases; α-MEM, α-minimum essential medium; PBS, phosphate-buffered saline; FBS, fetal bovine serum; OD, optical density; CPC, cetylpyridinium chloride; BCA, bicinchoninic acid; GAPDH, glyceraldehyde-3-phosphate dehydrogenase; AOD, average optical density; TBST, Tris-buffered saline containing 0.1% Tween 20; BSA, bovine serum albumin; DAPI, 4,6-diamidino-2-phenylindole; SD, Sprague-Dawley; SPF, specific pathogen-free; ROI, region of interest; BV/TV, bone volume/total volume; Tb.Th, trabecular thickness; Tb.Sp, trabecular separation/spacing; EDTA, Ethylenediaminetetraacetic acid; ANOVA, analysis of variance; hUCMSC, human umbilical cord mesenchymal stem cell; SFDA, State Food, and Drug Administration; OI, osteogenesis imperfecta; Sirt6, Sirtuin 6; FasL, FasrymndritFas Ligand.

Acknowledgments

This work was supported by the Province Natural Science Foundation of Shandong Province, grant number ZR2021QH340.

Disclosure

The authors report no conflicts of interest in this work.

References

1. Li XT, Tang Y, Huang XL, et al. Factors influencing subjective orthodontic treatment need and culture-related differences among Chinese natives and foreign inhabitants. *Int J Oral Sci*. 2010;2(3):149–157. doi:10.4248/IJOS10050
2. Li Y, Zhan Q, Bao M, et al. Biomechanical and biological responses of periodontium in orthodontic tooth movement: up-date in a new decade. *Int J Oral Sci*. 2021;13(1):20. doi:10.1038/s41368-021-00125-5
3. Asiry MA. Biological aspects of orthodontic tooth movement: a review of literature. *Saudi J Biol Sci*. 2018;25(6):1027–1032. doi:10.1016/j.sjbs.2018.03.008
4. Maltha JC, Kuijpers-Jagtman AM. Mechanobiology of orthodontic tooth movement: an update. *J World Fed Orthod*. 2023;12(4):156–160. doi:10.1016/j.ejwf.2023.05.001
5. Li Y, Jacox LA, Little SH, et al. Orthodontic tooth movement: the biology and clinical implications. *Kaohsiung J Med Sci*. 2018;34(4):207–214. doi:10.1016/j.kjms.2018.01.007
6. Seddiqi H, Klein-Nulend J, Jin J. Osteocyte mechanotransduction in orthodontic tooth movement. *Curr Osteoporosis Rep*. 2023;21(6):731–742. doi:10.1007/s11914-023-00826-2
7. Littlewood S, Kandasamy S, Huang G. Retention and relapse in clinical practice. *Aust Dent J*. 2017;62(S1):51–57.
8. Shanshan R, Xin D, Ming Y, et al. Factors affecting stability after fixed orthodontic treatment. *Chin J Stomatol*. 2018;53(9):599–603. doi:10.3760/cma.j.issn.1002-0098.2018.09.006
9. Maltha JC, Kuijpers-Jagtman AM, Von den Hoff JW, et al. Relapse revisited-animal studies and its translational application to the orthodontic office. *Semin Orthod*. 2017;23(4):390–398. doi:10.1053/j.sodo.2017.07.009
10. Franzen TJ, Monjo M, Rubert M, et al. Expression of bone markers and micro-CT analysis of alveolar bone during orthodontic relapse. *Orthod Craniofac Res*. 2014;17(4):249–258. doi:10.1111/ocr.12050
11. Rosyida NF, Ana ID, Alhasyimi AA. The use of polymers to enhance post-orthodontic tooth stability. Review. *Polymers*. 2023;15(1):14.103.
12. Fleming PS, Pandis N. Orthodontic retention: rationale and periodontal implications. *Periodontol*. 2024. doi:10.1111/prd.12560
13. Krämer A, Sjöström M, Apelthun C, et al. Post-treatment stability after 5 years of retention with vacuum-formed and bonded retainers—a randomized controlled trial. *Eur J Orthod*. 2023;45(1):68–78. doi:10.1093/ejo/cjac043
14. Liu Y, Zhang T, Zhang C, et al. Aspirin blocks orthodontic relapse via inhibition of CD4+ T lymphocytes. *J Dent Res*. 2017;96(5):586–594. doi:10.1177/0022034516685527
15. Zhang S, Liu J, Feng F, et al. Rational design of viscoelastic hydrogels for periodontal ligament remodeling and repair. *Acta Biomater*. 2024;174:69–90. doi:10.1016/j.actbio.2023.12.017
16. Li Z, Yu M, Jin S, et al. Stress distribution and collagen remodeling of periodontal ligament during orthodontic tooth movement. *Front Pharmacol*. 2019;10:1263. doi:10.3389/fphar.2019.01263
17. Seo B-M, Miura M, Gronthos S, et al. Investigation of multipotent postnatal stem cells from human periodontal ligament. *Lancet*. 2004;364(9429):149–155. doi:10.1016/S0140-6736(04)16627-0
18. Xu X-Y, Li X, Wang J, et al. Concise review: periodontal tissue regeneration using stem cells: strategies and translational considerations. *Stem Cells Transl Med*. 2019;8(4):392–403. doi:10.1002/sctm.18-0181
19. Li Q, Yang G, Li J, et al. Stem cell therapies for periodontal tissue regeneration: a network meta-analysis of preclinical studies. *Stem Cell Res Ther*. 2020;11(1):427. doi:10.1186/s13287-020-01938-7
20. Liu C, Ma R, Wang L, et al. Rehmanniae Radix in osteoporosis: a review of traditional Chinese medicinal uses, phytochemistry, pharmacokinetics and pharmacology. *J Ethnopharmacol*. 2017;198:351–362. doi:10.1016/j.jep.2017.01.021
21. Li M, Jiang H, Hao Y, et al. A systematic review on botany, processing, application, phytochemistry and pharmacological action of Radix Rehmnniae. *J Ethnopharmacol*. 2022;285:114820. doi:10.1016/j.jep.2021.114820

22. Xia B, Xu B, Sun Y, et al. The effects of Liuwei Dihuang on canonical Wnt/β-catenin signaling pathway in osteoporosis. *J Ethnopharmacol*. 2014;153(1):133–141. doi:10.1016/j.jep.2014.01.040
23. Gosset A, Pouillès J-M, Trémollieres F. Menopausal hormone therapy for the management of osteoporosis. *Best Pract Res Clin Endocrinol Metab*. 2021;35(6):101551.
24. Zhao L, Du W, Zhao D, et al. Catalpol protects against high glucose-induced bone loss by regulating osteoblast function. *Front Pharmacol*. 2021;12:626621. doi:10.3389/fphar.2021.626621
25. Zhu Y, Wang Y, Jia Y, et al. Catalpol promotes the osteogenic differentiation of bone marrow mesenchymal stem cells via the Wnt/β-catenin pathway. *Stem Cell Res Ther*. 2019;10(1):37. doi:10.1186/s13287-019-1143-y
26. Xu L, Xu G, Sun N, et al. Catalpol ameliorates dexamethasone-induced osteoporosis by promoting osteogenic differentiation of bone marrow mesenchymal stem cells via the activation of PKD1 promoter. *J Pharmacol Sci*. 2023;153(4):221–231. doi:10.1016/j.jphs.2023.10.002
27. Lai N, Zhang J, Ma X, et al. Regulatory effect of catalpol on Th1/Th2 cells in mice with bone loss induced by estrogen deficiency. *Am J Reprod Immunol*. 2015;74(6):487–498. doi:10.1111/aji.12423
28. Bhattamisra SK, Yap KH, Rao V, et al. Multiple biological effects of an iridoid glucoside, catalpol, and its underlying molecular mechanisms. *Biomolecules*. 2019;10(1):32. doi:10.3390/biom10010032
29. Di Naro E, Loverro M, Converti I, et al. The effect of menopause hypoestrogenism on osteogenic differentiation of periodontal ligament cells (PDLC) and stem cells (PDLCs): a systematic review. *Rev Healthcare*. 2021;9(5):11.572.
30. Deng L, Guo Y. Estrogen effects on orthodontic tooth movement and orthodontically-induced root resorption. *Arch Oral Biol*. 2020;118:104840. doi:10.1016/j.archoralbio.2020.104840
31. Xu K, Sha YQ, Wang SX, et al. Effects of Bakuchiol on chondrocyte proliferation via the PI3K-Akt and ERK1/2 pathways mediated by the estrogen receptor for promotion of the regeneration of knee articular cartilage defects. *Cell Prolif*. 2019;52(5):11.e12666. doi:10.1111/cpr.12666
32. Chen S, Jin J, Xu Z, et al. Catalpol attenuates osteoporosis in ovariectomized rats through promoting osteoclast apoptosis via the Sirt6-ERα-FasL axis. *Phytomedicine*. 2024;123:155262. doi:10.1016/j.phymed.2023.155262
33. Clusan L, Ferrière F, Flouriot G, et al. A basic review on estrogen receptor signaling pathways in breast cancer. *Int J Mol Sci*. 2023;24(7):6834. doi:10.3390/ijms24076834
34. Deng R-M, Zhou J. The role of PI3K/AKT signaling pathway in myocardial ischemia-reperfusion injury. *Int Immunopharmacol*. 2023;123:110714. doi:10.1016/j.intimp.2023.110714
35. Shim NY, Ryu JI, Heo JS. Osteoinductive function of fucoidan on periodontal ligament stem cells: role of PI3K/Akt and Wnt/β-catenin signaling pathways. *Oral Dis*. 2022;28(6):1628–1639. doi:10.1111/odi.13829
36. Yan Y, Zhang H, Liu L, et al. Periostin reverses high glucose-inhibited osteogenesis of periodontal ligament stem cells via AKT pathway. *Life Sci*. 2020;242:117184. doi:10.1016/j.lfs.2019.117184
37. Faraldi M, Mangiavini L, Conte C, et al. A novel methodological approach to simultaneously extract high-quality total RNA and proteins from cortical and trabecular bone. *Open Biol*. 2022;12(5):210387. doi:10.1098/rsob.210387
38. Livak KJ, Schmittgen TD. Analysis of relative gene expression data using real-time quantitative PCR and the 2−ΔΔCT method. *Methods*. 2001;25(4):402–408. doi:10.1006/meth.2001.1262
39. Zhao R, Tao L, Qiu S, et al. Melatonin rescues glucocorticoid-induced inhibition of osteoblast differentiation in MC3T3-E1 cells via the PI3K/AKT and BMP/Smad signalling pathways. *Life Sci*. 2020;257:118044. doi:10.1016/j.lfs.2020.118044
40. Sun B, Xiao J, Sun XB, et al. Notoginsenoside R1 attenuates cardiac dysfunction in endotoxemic mice: an insight into estrogen receptor activation and PI3K/Akt signaling. *Br J Pharmacol*. 2013;168(7):1758–1770. doi:10.1111/bph.12063
41. Wan Mohammad WMZ. Sample size calculation in animal studies using resource equation approach. *Malays J Med Sci*. 2017;24(5):101–105. doi:10.21315/mjms2017.24.5.11
42. Zou J-H, Chen F, Li Y-L, et al. Effects of green tea extract epigallocatechin-3-gallate (EGCG) on orthodontic tooth movement and root resorption in rats. *Arch Oral Biol*. 2023;150:105691. doi:10.1016/j.archoralbio.2023.105691
43. Li H, Li Y, Zou J, et al. Sinomenine inhibits orthodontic tooth movement and root resorption in rats and enhances osteogenic differentiation of PDLSCs. *Drug Des Devel Ther*. 2022;16:2949–2965. doi:10.2147/DDDT.S379468
44. Yang F, Wang XX, Ma D, et al. Effects of triptolide on tooth movement and root resorption in rats. *Drug Des Devel Ther*. 2019;13:3963–3975. doi:10.2147/DDDT.S217936
45. Angjelova A, Jovanova E, Polizzi A, et al. Insights and advancements in periodontal tissue engineering and bone regeneration. *Medicina*. 2024;60(5):773. doi:10.3390/medicina60050773
46. Liu J, Ruan J, Weir MD, et al. Periodontal bone-ligament-cementum regeneration via scaffolds and stem cells. *Cells*. 2019;8(6):537. doi:10.3390/cells8060537
47. Shuo YA, Biao ZH, Tian XY, et al. Exosomes derived from human umbilical cord mesenchymal stem cells enhance the osteoblastic differentiation of periodontal ligament stem cells under high Glucose conditions through the PI3K/AKT signaling pathway. *Biomed Environ Sci*. 2022;35(9):811–820. doi:10.3967/bes2022.105
48. Han Y, Wang X, Ma D, et al. Ipriflavone promotes proliferation and osteogenic differentiation of periodontal ligament cells by activating GPR30/PI3K/AKT signaling pathway. *Drug Des Devel Ther*. 2018;12:137–148. doi:10.2147/DDDT.S148457
49. Marjoribanks J, Farquhar C, Roberts H, et al. Long-term hormone therapy for perimenopausal and postmenopausal women. *Cochrane Database Syst Rev*. 2017;1(1):CD004143. doi:10.1002/14651858.CD004143.pub5
50. Cho L, Kaunitz AM, Faubion SS, et al. Rethinking menopausal hormone therapy: for whom, what, when, and how long? *Circulation*. 2023;147(7):597–610. doi:10.1161/CIRCULATIONAHA.122.061559
51. Chen L, Zhang RY, Xie J, et al. STAT3 activation by catalpol promotes osteogenesis-angiogenesis coupling, thus accelerating osteoporotic bone repair. *Stem Cell Res Ther*. 2021;12(1):108. doi:10.1186/s13287-021-02178-z
52. Liu J, Zhao Z, Ruan J, et al. Stem cells in the periodontal ligament differentiated into osteogenic, fibrogenic and cementogenic lineages for the regeneration of the periodontal complex. *J Dent*. 2020;92:103259. doi:10.1016/j.jdent.2019.103259
53. Vimalraj S. Alkaline phosphatase: structure, expression and its function in bone mineralization. Review. *Gene*. 2020;754:8.144855. doi:10.1016/j.gene.2020.144855

54. Hald JD, Folkestad L, Harsløf T, et al. Skeletal phenotypes in adult patients with osteogenesis imperfecta-correlations with COL1A1/COL1A2 genotype and collagen structure. *Osteoporos Int*. 2016;27(11):3331–3341. doi:10.1007/s00198-016-3653-0
55. Komori T. Regulation of proliferation, differentiation and functions of osteoblasts by Runx2. *Int J Mol Sci*. 2019;20(7):1694. doi:10.3390/ijms20071694
56. Vimalraj S, Arumugam B, Miranda PJ, et al. Runx2: structure, function, and phosphorylation in osteoblast differentiation. *Int J Biol Macromol*. 2015;78:202–208. doi:10.1016/j.ijbiomac.2015.04.008
57. Calabrese EJ. Human periodontal ligament stem cells and hormesis: enhancing cell renewal and cell differentiation. *Pharmacol Res*. 2021;173:105914. doi:10.1016/j.phrs.2021.105914
58. Zhang Y, Cao XY, Li PF, et al. PSMC6 promotes osteoblast apoptosis through inhibiting PI3K/AKT signaling pathway activation in ovariectomy-induced osteoporosis mouse model. *J Cell Physiol*. 2020;235(7–8):5511–5524. doi:10.1002/jcp.29261
59. Choi YH, Kim YJ, Jeong HM, et al. Akt enhances Runx2 protein stability by regulating Smurf2 function during osteoblast differentiation. *FEBS J*. 2014;281(16):3656–3666. doi:10.1111/febs.12887
60. Mukherjee A, Rotwein P. Akt promotes BMP2-mediated osteoblast differentiation and bone development. *J Cell Sci*. 2009;122(5):716–726. doi:10.1242/jcs.042770
61. Xiong YX, Zhao B, Zhang WJ, et al. Curcumin promotes osteogenic differentiation of periodontal ligament stem cells through the PI3K/AKT/Nrf2 signaling pathway. *Iran J Basic Med Sci*. 2020;23(7):954–960. doi:10.22038/IJBMS.2020.44070.10351
62. Pan F, Zhang R, Wang G, et al. Estrogen receptors are involved in the osteogenic differentiation of periodontal ligament stem cells. *Biosci Rep*. 2011;31(2):117–124. doi:10.1042/BSR20100029
63. Quast A, Martian V, Bohnsack A, et al. Donor variation and sex hormone receptors in periodontal ligament cells. *Arch Oral Biol*. 2021;122:105026. doi:10.1016/j.archoralbio.2020.105026
64. Wu G-J, Chen J-T, Cherng Y-G, et al. Genistein improves bone healing via triggering estrogen receptor alpha-mediated expressions of osteogenesis-associated genes and consequent maturation of osteoblasts. *J Agric Food Chem*. 2020;68(39):10639–10650. doi:10.1021/acs.jafc.0c02830
65. Moon YJ, Zhang Z, Bang IH, et al. Sirtuin 6 in preosteoclasts suppresses age- and estrogen deficiency-related bone loss by stabilizing estrogen receptor α. *Cell Death Differ*. 2019;26(11):2358–2370. doi:10.1038/s41418-019-0306-9
66. Takegahara N, Kim H, Choi Y. Unraveling the intricacies of osteoclast differentiation and maturation: insight into novel therapeutic strategies for bone-destructive diseases. *Exp Mol Med*. 2024;56(2):264–272. doi:10.1038/s12276-024-01157-7
67. Meng J, Zhang W, Wang C, et al. Catalpol suppresses osteoclastogenesis and attenuates osteoclast-derived bone resorption by modulating PTEN activity. *Biochem Pharmacol*. 2020;171:113715. doi:10.1016/j.bcp.2019.113715
68. Florencio-Silva R, Sasso GRDS, Sasso-Cerri E, et al. Biology of bone tissue: structure, function, and factors that influence bone cells. *Biomed Res Int*. 2015;2015:1–17. doi:10.1155/2015/421746
69. Scribante A, Gallo S, Pascadopoli M, et al. Ozonized gels vs chlorhexidine in non-surgical periodontal treatment: a randomized clinical trial. *Oral Dis*. 2024;30(6):3993–4000. doi:10.1111/odi.14829
70. Elbay M, Elbay ÜŞ, Kaya E, et al. Effects of photobiomodulation with different application parameters on injection pain in children: a randomized clinical trial. *J Clin Pediatr Dent*. 2023;47(4):54–62. doi:10.22514/jocpd.2023.035
71. Butera A, Pascadopoli M, Nardi MG, et al. Clinical use of paraprobiotics for pregnant women with periodontitis: randomized clinical trial. *Dent J*. 2024;12(4):116. doi:10.3390/dj12040116